

1 Assessing the relationship of ancient and modern populations

2 Joshua G. Schraiber

3 Started on October 22, 2016. Compiled on March 3, 2017

4 **Abstract**

5 Genetic material sequenced from ancient samples is revolutionizing our understand-
6 ing of the recent evolutionary past. However, ancient DNA is often degraded, resulting
7 in low coverage, error-prone sequencing. Several solutions exist to this problem, rang-
8 ing from simple approach such as selecting a read at random for each site to more
9 complicated approaches involving genotype likelihoods. In this work, we present a
10 novel method for assessing the relationship of an ancient sample with a modern pop-
11 ulation while accounting for sequencing error by analyzing raw read from multiple
12 ancient individuals simultaneously. We show that when analyzing SNP data, it is bet-
13 ter to sequencing more ancient samples to low coverage: two samples sequenced to
14 0.5x coverage provide better resolution than a single sample sequenced to 2x coverage.
15 We also examined the power to detect whether an ancient sample is directly ancestral
16 to a modern population, finding that with even a few high coverage individuals, even
17 ancient samples that are very slightly diverged from the modern population can be de-
18 tected with ease. When we applied our approach to European samples, we found that
19 no ancient samples represent direct ancestors of modern Europeans. We also found
20 that, as shown previously, the most ancient Europeans appear to have had the small-
21 est effective population sizes, indicating a role for agriculture in modern population
22 growth.

1 Introduction

Ancient DNA (aDNA) is now ubiquitous in population genetics. Advances in DNA isolation [Dabney et al., 2013], library preparation [Meyer et al., 2012], bone sampling [Pinhasi et al., 2015], and sequence capture Haak et al. [2015] make it possible to obtain genome-wide data from hundreds of samples [Haak et al., 2015, Mathieson et al., 2015, Allentoft et al., 2015, Fu et al., 2016]. Analysis of these data can provide new insight into recent evolutionary processes which leave faint signatures in modern genomes, including natural selection [Schraiber et al., 2016, Jewett et al., 2016] and population replacement [Sjödín et al., 2014, Lazaridis et al., 2014].

One of the most powerful uses of ancient DNA is to assess the continuity of ancient and modern populations. In many cases, it is unclear whether populations that occupied an area in the past are the direct ancestors of the current inhabitants of that area. However, this can be next to impossible to assess using only modern genomes. Questions of population continuity and replacement have particular relevance for the spread of cultures and technology in humans [Lazaridis et al., 2016]. For instance, recent work showed that modern Native Americans are directly descended from the Clovis culture that inhabited North America over 10,000 years ago, settling a long-standing debate about the colonization of the Americas [Rasmussen et al., 2014].

Despite its utility in addressing difficult-to-answer questions in evolutionary biology, aDNA also has several limitations. Most strikingly, DNA decays rapidly following the death of an organism, resulting in highly fragmented, degraded starting material when sequencing [Sawyer et al., 2012]. Thus, ancient data is frequently sequenced to low coverage and has a significantly higher base-calling error rate than modern samples. When working with diploid data, as in aDNA extracted from plants and animals, the low coverage prevents genotypes from being called with confidence.

Several strategies are commonly used to address the low-coverage data. One of the most common approaches is to sample a random read from each covered site and use that as a haploid genotype call [Haak et al., 2015, Mathieson et al., 2015, Allentoft

et al., 2015, Fu et al., 2016, Lazaridis et al., 2016]. Many common approaches to the analyses of ancient DNA, such as the usage of F-statistics [Patterson et al., 2012], are designed with this kind of dataset in mind. As shown by Peter [2016], F-statistics can be interpreted as linear combinations of simpler summary statistics and can often be understood in terms of testing a tree-like structure relating populations. Nonetheless, despite the simplicity and appeal of this approach, it has several drawbacks. Primarily, it throws away reads from sites that are covered more than once, resulting in a potential loss of information from expensive, difficult-to-acquire data. These approach are also strongly impacted by sequencing error and contamination.

On the other hand, several approaches exist to either work with genotype likelihoods or the raw read data. Genotype likelihoods are the probabilities of the read data at a site given each of the three possible diploid genotypes at that site. They can be used in calculation of population genetic statistics or likelihood functions to average over uncertainty in the genotype [Korneliussen et al., 2014]. However, many such approaches assume that genotype likelihoods are fixed by the SNP calling algorithm. However, with low coverage data, an increase in accuracy is expected if genotype likelihoods are co-estimated with other parameters of interest, due to the covariation between processes that influence read quality and genetic diversity, such as contamination.

A recent method that coestimates demographic parameters along with error and contamination rates by using genotype likelihoods showed that there can be significant power to assess the relationship of a single ancient sample to a modern population [Racimo et al., 2016]. Nonetheless, they found that for very low coverage data, inferences were not reliable. Thus, they were unable to apply their method to the large number of extremely low coverage ($< 1x$) genomes that are available. Moreover, they were unable to explore the tradeoffs that come with a limited budget: can we learn more by sequencing fewer individuals to high coverage, or more individuals at lower coverage?

Here, we develop a novel maximum likelihood approach for analyzing low coverage ancient DNA in relation to a modern population. We work directly with raw read data

and explicitly model base-calling errors. Crucially, our approach incorporates data from multiple individuals that belong to the same ancient population, which we show substantially increases power and reduces error in parameter estimates. We then apply our new methodology to ancient human data, and show that we can perform accurate demographic inference even from very low coverage samples by analyzing them jointly.

2 Results

2.1 Sampling alleles in ancient populations

We assume a scenario in which allele frequencies are known with high accuracy in a modern population. Suppose that an allele is known to be at frequency $x \in (0, 1)$ in the modern population, and we wish to compute the probability of obtaining k copies of that allele in a sample of n ($0 \leq k \leq n$) chromosomes from an ancient population. Conditioning on the frequency of the allele in the modern population minimizes the impact of ascertainment, and allows this approach to be used for SNP capture data.

To calculate the sampling probability, we assume a simple demographic model in which the ancient individual belongs to a population that split off from the modern population τ_1 generations ago, and subsequently existed as an isolated population for τ_2 generations. Further, we assume that the modern population has effective size $N_e^{(1)}$ and that the ancient population has effective size $N_e^{(2)}$, and measure time in diffusion units, $t_i = \tau_i / (2N_e^{(i)})$. If we know the conditional probability that an allele is at frequency y in the ancient sample, given that it is at frequency x , denoted $f(y; x, t_1, t_2)$, then the sampling probability is simply an integral,

$$\begin{aligned} P_{n,k}(x) &= \int_0^1 \binom{n}{k} y^k (1-y)^{n-k} f(y; x, t_1, t_2) dy \\ &= \binom{n}{k} \mathbb{E}_x (Y^k (1-Y)^{n-k}; t_1, t_2) \\ &\equiv \binom{n}{k} p_{n,k}(t_1, t_2) \end{aligned} \tag{1}$$

93 Thus, we must compute the binomial moments of the allele frequency distribution in
94 the ancient population. In the Methods, we show that this can be computed using
95 matrix exponentiation,

$$p_{n,k}(t_1, t_2) = \left(e^{Qt_2} e^{Q^\perp t_1} \mathbf{h}_n \right)_i, \quad (2)$$

96 where $(\mathbf{v})_i$ indicates the i th element of the vector \mathbf{v} , $\mathbf{h}_n = ((1-x)^n, x(1-x)^{n-1}, \dots, x^n)^T$
97 and Q and Q^\perp are the sparse matrices

$$Q_{ij} = \begin{cases} \frac{1}{2}i(i-1) & \text{if } j = i-1 \\ -i(n-i) & \text{if } j = i \\ \frac{1}{2}(n-i)(n-i-1) & \text{if } j = i+1 \\ 0 & \text{else} \end{cases}$$

98 and

$$Q^\perp_{ij} = \begin{cases} \frac{1}{2}i(i-1) & \text{if } j = i-1 \\ -i(n-i+1) & \text{if } j = i \\ \frac{1}{2}(n-i+1)(n-i) & \text{if } j = i+1 \\ 0 & \text{else.} \end{cases}$$

99 This result has an interesting interpretation: the matrix Q^\perp can be thought of as
100 evolving the allele frequencies back in time from the modern population to the common
101 ancestor of the ancient and modern populations, while Q evolves the allele frequencies
102 forward in time from the common ancestor to the ancient population (Fig 1).

103 [Figure 1 about here.]

104 Because of the fragmentation and degradation of DNA that is inherent in obtaining
105 sequence data from ancient individuals, it is difficult to obtain the high coverage data
106 necessary to make high quality genotype calls from ancient individuals. To address this,
107 we instead work directly with raw read data, and average over all the possible genotypes
108 weighted by their probability of producing the data. Specifically, we follow Nielsen et al.

[2012] in modeling the probability of the read data in the ancient population, given the allele frequency at site l as

$$\mathbb{P}(R_l|k) = \sum_{g_{1,l}=0}^2 \dots \sum_{g_{n,l}=0}^2 \mathbb{I}\left(\sum_{i=1}^n g_{i,l} = k\right) \prod_{i=1}^n \binom{2}{g_{i,l}} \mathbb{P}(R_{i,l}|g_{i,l}),$$

where $R_{i,l} = (a_{i,l}, d_{i,l})$ are the counts of ancestral and derived reads in individual i at site l , $g_{i,l} \in \{0, 1, 2\}$ indicates the possible genotype of individual i at site l (i.e. 0 = homozygous ancestral, 1 = heterozygous, 2 = homozygous derived), and $\mathbb{P}(R_{i,l}|g_{i,l})$ is the probability of the read data at site l for individual i , assuming that the individual truly has genotype $g_{i,l}$. We use a binomial sampling with error model, in which the probability that a truly derived site appears ancestral (and vice versa) is given by ϵ . Thus,

$$\mathbb{P}(R|g) = \binom{a+d}{d} p_g^d (1-p_g)^a$$

with

$$\begin{aligned} p_0 &= \epsilon \\ p_1 &= \frac{1}{2} \\ p_2 &= 1 - \epsilon \end{aligned}$$

.

Combining these two aspects together by summing over possible allele frequencies weighted by their probabilities, we obtain our likelihood of the ancient data,

$$L(D) = \prod_{l=1}^L \sum_{k=0}^n \mathbb{P}(R_l|k) p_{n,k}(x_l). \quad (3)$$

2.2 Impact of coverage and number of samples on inferences

To explore the tradeoff of sequencing more individuals at lower depth compared to fewer individuals at higher coverage, we performed simulations using `msprime` [Kelleher et al., 2016] combined with custom scripts to simulate base calling error and low coverage data. First, we examined the impact of coverage and number of samples on the ability to recover the drift times in the modern and the ancient populations. Figure 2 shows results for data simulated with $t_1 = 0.02$ and $t_2 = 0.05$, corresponding to an ancient individual who died 300 generations ago from population of effective size 1000. The populations split 400 generations ago, and the modern population has an effective size of 10000. We simulated approximately 180000 SNPs by simulating 100000 500 base pair fragments. Inferences of t_1 can be relatively accurate even with only one low coverage ancient sample (Figure 2A). However, inferences of t_2 benefit much more from increasing the number of ancient samples, as opposed to coverage (Figure 2B). In particular, two individuals sequenced to 0.5x coverage have a much lower error than a single individual sequenced to 2x coverage. To explore this effect further, we derived the sampling probability of alleles covered by exactly one sequencing read (see Methods). We found that sites covered only once have no information about t_2 , suggesting that evidence of heterozygosity is very important for inferences about t_2 .

[Figure 2 about here.]

We next examined the impact of coverage and sampling on the power to reject the hypothesis that the ancient individuals came from a population that is directly ancestral to the modern population. We analyzed both low coverage (0.5x) and higher coverage (4x) datasets consisting of 1 (for both low and high coverage samples) or 5 individuals (only for low coverage). We simulated data with parameters identical to the previous experiment, except we now examined the impact of varying the age of the ancient sample from 0 generations ago through to the split time with the modern population. We then performed a likelihood ratio test comparing the null model of continuity, in which $t_2 = 0$, to a model in which the ancient population is not continuous.

Figure 3 shows the power of the likelihood ratio test. For a single individual sequenced to low coverage, we see that the test only has power for very recently sampled ancient individuals (i.e. samples that are highly diverged from the modern population). However, the power increases dramatically as the number of individuals or the coverage per individual is increased; sequencing 5 individuals to 0.5x coverage results in essentially perfect power to reject continuity. Nonetheless, for samples that are very close to the divergence time, it will be difficult to determine if they are ancestral to the modern population or not, because differentiation is incomplete.

[Figure 3 about here.]

2.3 Application to ancient humans

We applied our approach to ancient human data from Mathieson et al. [2015], which is primarily derived from a SNP capture approach that targeted 1.2 million SNPs. Based on sampling location and associated archeological materials, the individuals were grouped into *a priori* panels, which we used to specify population membership when analyzing individuals together. We analyzed all samples for their relationship to the CEU individuals from the 1000 Genomes Project [Consortium, 2015]. Based on our results that suggested that extremely low coverage samples would yield unreliable estimates, we excluded panels that are composed of only a single individual sequenced to less than 2x coverage.

We computed maximum likelihood estimates of t_1 and t_2 for individuals as grouped into populations (Figure 4A; Table 1). We observe that t_2 is significantly greater than 0 for all populations. Thus, none of these populations are consistent with directly making up a large proportion of the ancestry of modern CEU individuals. Strikingly, we see that $t_2 \gg t_1$, despite the fact that the ancient samples must have existed for fewer generations since the population split than the modern samples. This suggests that all of the ancient populations are characterized by extremely small effective population sizes.

[Table 1 about here.]

[Figure 4 about here.]

We further explored the relationship between the dates of the ancient samples and the parameters of the model by plotting t_1 and t_2 against the mean sample date of all samples in that population (Figure 4B, C). We expected to find that t_1 correlated with sample age, under the assumption that samples were members of relatively short-lived populations that diverged from the “main-stem” of CEU ancestry. Instead, we see no correlation between t_1 and sample time, suggesting that the relationship of these populations to the CEU is complicated and not summarized well by the age of the samples. On the other hand, we see a strong positive correlation between t_2 and sampling time ($p < 1 \times 10^{-4}$). Because t_2 is a compound parameter, it is difficult to directly interpret this relationship. However, it is consistent with the most ancient samples belonging to populations with the smallest effective sizes, consistent with previous observations [Skoglund et al., 2014].

Our model provided estimates of sequencing error in each of our analyzed ancient individuals. We found that almost all analyzed individuals had inferred error rates less than 1%, with many individuals clustering near 0.5% error (Figure 5A). We hypothesized that higher coverage individuals may have lower error rates, because high coverage may indicate better preserved DNA. We found a marginally significant negative correlation between the log of the error rate and the log of coverage when two outlier individuals with inferred error rates of 0% were excluded ($p = 0.06$, Figure 5B).

[Figure 5 about here.]

Finally, we examined the impact of grouping individuals into populations in real data. We see that estimates of t_1 for low coverage samples are typically lower when analyzed individually than when pooled with other individuals of the same panel (Figure 6A), suggesting a slightly downward bias in estimating t_1 for low coverage samples. On the other hand, there is substantial bias toward overestimating t_2 when analyzing sam-

ples individually, particularly for very low coverage samples (Figure 6B). This again shows that for estimates that rely on heterozygosity in ancient populations, pooling many low coverage individuals can significantly improve estimates.

[Figure 6 about here.]

3 Discussion

Ancient DNA (aDNA) presents unique opportunities to enhance our understanding of demography and selection in recent history. However, it also comes equipped with several challenges, due to postmortem DNA damage [Sawyer et al., 2012]. Several strategies have been developed to deal with the low quality of aDNA data, from relatively simple options like sampling a read at random at every site [Green et al., 2010] to more complicated methods making use of genotype likelihoods [Racimo et al., 2016]. Here, we presented a novel maximum likelihood approach for making inferences about how ancient populations are related to modern populations by analyzing read counts from multiple ancient individuals and explicitly modeling relationship between the two populations. Using this approach, we examined some aspects of sampling strategy for aDNA analysis and we applied our approach to ancient humans.

We found that sequencing many individuals from an ancient population to low coverage (.5-1x) can be a significantly more cost effective strategy than sequencing fewer individuals to relatively high coverage. For instance, we saw from simulations that far more accurate estimates of the drift time in an ancient population can be obtained by pooling 2 individuals at 0.5x coverage than by sequencing a single individual to 2x coverage (Figure 2). We saw this replicated in our analysis of the real data: low coverage individuals showed a significant amount of variation and bias in estimating the model parameters that was substantially reduced when individuals were analyzed jointly in a population (Figure 6). To explore this further, we showed that sites sequenced to 1x coverage in a single individual retain no information about the drift time in the ancient population. This can be intuitively understood because the drift time in the ancient

population is strongly related the amount of heterozygosity in the ancient population: an ancient population with a longer drift time will have lower heterozygosity at sites shared with a modern population. When a site is only sequenced once in a single individual, there is no information about the heterozygosity of that site. We also observed a pronounced upward bias in estimates of the drift time in the ancient population from low coverage samples. We speculate that this is due to the presence of few sites covered more than once being likely to be homozygous, thus deflating the estimate of heterozygosity in the ancient population. Thus, for analysis of SNP data, we recommend that aDNA sampling be conducted to maximize the number of individuals from each ancient population that can be sequenced to $\sim 1\times$, rather than attempting to sequence fewer individuals to high coverage.

Of particular interest in many studies of ancient populations is the question of direct ancestry: are the ancient samples members of a population that contributed substantially to a modern population? Several methods have been proposed to test this question, but thus far they have been limited to many individuals sequenced at a single locus [Sjödín et al., 2014] or to a single individual with genome-wide data [Rasmussen et al., 2014]. Our approach provides a rigorous, maximum likelihood framework for testing questions of population continuity using multiple low coverage ancient samples. We saw from simulations (Figure 3) that data from single, low coverage individuals result in very little power to reject the null hypothesis of continuity unless the ancient sample is very recent (i.e. it has been diverged from the modern population for a long time). Nonetheless, when low coverage individuals are pooled together, or a single high coverage individual is used, there is substantial power to reject continuity for all but the most ancient samples (i.e. samples dating from very near the population split time).

When we applied our approach to European history, we made several noteworthy observations. Primarily, we rejected continuity for all populations that we analyzed, suggesting that most ancient samples thus far collected come from populations that had diverged from main-stem European ancestry, and did not contribute a substantial

portion of ancestry directly to modern Europeans. Secondly, we observed that the drift time in the ancient population was much larger than the drift time in the modern population. This supports the observation that ancient Europeans were often members of small, isolated populations [Skoglund et al., 2014]. We obtained further support for this by examining the relationship between the age of the ancient populations and the drift time leading to them (Figure 4C). We saw a strong positive correlation, and although this drift time is a compound parameter, which complicates interpretations, it appears that the oldest Europeans were members of extremely small populations, and that effective population size has grown through time as agriculture spread through Europe.

We anticipate the further development of methods that explicitly account for differential drift times in ancient and modern samples will become important as aDNA research becomes even more integrating into population genomics. This is because many common summary methods, such as the use of Structure [Pritchard et al., 2000] and Admixture [Alexander et al., 2009], are sensitive to differential amounts of drift between populations [Falush et al., 2016]. As we've shown in ancient Europeans, ancient samples tend to come from isolated subpopulations with a large amount of drift, thus confounding such summary approaches. Moreover, standard population genetics theory shows that allele frequencies are expected to be deterministically lower in ancient samples, even if they are direct ancestors of a modern population. Intuitively, this arises because the alleles must have arisen at some point from new mutations, and thus were at lower frequencies in the past. A potentially fruitful avenue to combine these approaches moving forward may be to separate regions of the genome based on ancestry components, and assess the ancestry of ancient samples relative to specific ancestry components, rather than to genomes as a whole.

Our current approach leaves several avenues for improvement. Although our method is robust to non-constant demography because we consider only alleles that are segregating in both the modern and the ancient population, we are losing information by not modeling new mutations that arise in the ancient population. Similarly, we

only consider a single ancient population at a time, albeit with multiple samples. Ideally, ancient samples would be embedded in complex demographic models that include admixture, detailing their relationships to each other and to modern populations [Patterson et al., 2012, Lipson and Reich, 2017]. However, inference of such complex models is difficult, and though there has been some progress in simplified cases [Lipson et al., 2014, Pickrell and Pritchard, 2012], it remains an open problem due to the difficulty of simultaneously inferring a non-tree-like topology along with demographic parameters. Software such as *mom* [Kamm et al., 2016] that can compute the likelihood of SNP data in an admixture graph may be able to be used to integrate over genotype uncertainty in larger settings than considered here.

4 Methods

4.1 Computing allele frequency moments in the ancient population

We wish to compute moments of the form

$$\mathbb{E}_x(g(Y); t_1, t_2) = \int_0^1 g(y)f(y; x, t_1, t_2)dy. \quad (4)$$

To do so, we make use of several results from diffusion theory. To ensure that this paper is self contained, we briefly review those results here. The interested reader may find much of this material covered in Ewens [2012], Karlin and Taylor [1981]. Several similar calculations can be found in Griffiths [2003].

Let the probability of an allele going from frequency x to frequency y in τ generations in a population of size N_e be $f(x, y; t)$, where $t = \tau/(2N_e)$. Under a wide variety of models, the change in allele frequencies through time is well approximated by the Wright-Fisher diffusion, which is characterized by its generator,

$$\mathcal{L} = \frac{1}{2}x(1-x)\frac{d^2}{dx^2}.$$

310 The generator of a diffusion process is useful, because it can be used to define a differ-
311 ential equation for the moments of that process,

$$\frac{d}{dt}\mathbb{E}_x(g(X_t)) = \mathbb{E}_x(\mathcal{L}g(X_t)). \quad (5)$$

312 We will require the *speed measure* of the Wright-Fisher diffusion, $m(x) = x^{-1}(1 -$
313 $x)^{-1}$, which essentially describes how slow a diffusion at position x is “moving” com-
314 pared to a Brownian motion at position x . Note that all diffusions are reversible with
315 respect to their speed measures, i.e.

$$m(x)f(x, y; t) = m(y)f(y, x; t).$$

316 We additionally require the probability of loss, i.e. the probability that the allele
317 currently at frequency x is ultimately lost from the population. This is

$$u_0(x) = 1 - x.$$

318 Note that it is possible to condition the Wright-Fisher diffusion to eventually be lost.
319 The transition density can be computed as

$$f^\downarrow(x, y; t) = f(x, y; t) \frac{u_0(y)}{u_0(x)}$$

320 by using Bayes theorem. The diffusion conditioned on loss is characterized by its
321 generator,

$$\mathcal{L}^\downarrow = -x \frac{d}{dx} + \frac{1}{2}x(1-x) \frac{d^2}{dx^2}.$$

322 In an infinite sites model, in which mutations occur at the times of a Poisson
323 process with rate $\theta/2$ and then each drift according to the Wright-Fisher diffusion, a
324 quasi-equilibrium distribution will be reached, known as the frequency spectrum. The
325 frequency spectrum, $\phi(x)$, predicts the number of sites at frequency x , and can be

326 written in terms of the speed measure and the probability of loss,

$$\phi(x) = \theta m(x) u_0(x).$$

327 To proceed with calculating (4), note that the conditional probability of an allele
328 being at frequency y in the ancient population given that it's at frequency x in the
329 modern population can be calculated

$$f(y; x, t_1, t_2) = \frac{f(x, y; t_1, t_2)}{\phi(x)}$$

330 where $f(x, y; t_1, t_2)$ is the joint probability of the allele frequencies in the modern and
331 ancient populations and $\phi(x)$ is the frequency spectrum in the modern population.

332 Assuming that the ancestral population of the modern and ancient samples was at
333 equilibrium, the joint distribution of allele frequencies can be computed by sampling
334 alleles from the frequency spectrum of the ancestor and evolving them forward in time
335 via the Wright-Fisher diffusion. This can be written mathematically as

$$f(x, y; t_1, t_2) = \int_0^1 f(z, x; t_1) f(z, y; t_2) \phi(z) dz.$$

We now expand the frequency spectrum in terms of the speed measure and the probability of loss and use reversibility with respect to the speed measure to rewrite the equation,

$$\begin{aligned} \int_0^1 f(z, x; t_1) f(z, y; t_2) \phi(z) dz &= \theta \int_0^1 f(z, x; t_1) f(z, y; t_2) m(z) u_0(z) dz \\ &= \theta \int_0^1 \frac{m(x)}{m(z)} f(x, z; t_1) f(z, y; t_2) m(z) u_0(z) dz \\ &= \theta m(x) u_0(x) \int_0^1 f(x, z; t_1) \frac{u_0(z)}{u_0(x)} f(z, y; t_2) dz \\ &= \phi(x) \int_0^1 f^\downarrow(x, z; t_1) f(z, y; t_2) dz. \end{aligned}$$

336 The third line follows by multiplying by $u_0(x)/u_0(x) = 1$. This equation has the inter-
 337 pretation of sampling an allele from the frequency spectrum in the modern population,
 338 then evolving it *backward* in time to the common ancestor, before evolving it *forward*
 339 in time to the ancient population. The interpretation of the diffusion conditioned on
 340 loss as evolving backward in time arises by considering the fact that alleles arose from
 341 unique mutations at some point in the past; hence, looking backward, alleles must
 342 eventually be lost at some point in the past.

To compute the expectation, we substitute this form for the joint probability into (4),

$$\begin{aligned} \int_0^1 g(y) f(y; x, t_1, t_2) dy &= \int_0^1 g(y) \left(\int_0^1 f^\downarrow(x, z; t_1) f(z, y; t_2) dz \right) dy \\ &= \int_0^1 \left(\int_0^1 g(y) f(z, y; t_2) dy \right) f^\downarrow(x, z; t_1) dz, \end{aligned}$$

where the second line follows by rearranging terms and exchanging the order of integration. Note that this formula takes the form of nested expectations. Specifically,

$$\begin{aligned} \int_0^1 g(y) f(z, y; t_2) dy &= \mathbb{E}_z(g(Y_{t_2})) \\ &\equiv h(z) \end{aligned}$$

and

$$\begin{aligned} \int_0^1 h(z) f^\downarrow(x, z; t_1) dz &= \mathbb{E}_x^\downarrow(h(Z_{t_1})) \\ &= \mathbb{E}_x(g(Y); t_1, t_2). \end{aligned}$$

343 We now use (5) to note that

$$\frac{d}{dt} p_{n,k} = \frac{k(k-1)}{2} p_{n,k-1} - k(n-k) p_{n,k} + \frac{(n-k)(n-k-1)}{2} p_{n,k+1}$$

344 and

$$\frac{d}{dt}p_{n,k}^\downarrow = \frac{k(k-1)}{2}p_{n,k-1}^\downarrow - k(n-k+1)p_{n,k}^\downarrow + \frac{(n-k+1)(n-k)}{2}p_{n,k+1}^\downarrow$$

345 with obvious boundary conditions $p_{n,k}(0; z) = z^k(1-z)^{n-k}$ and $p_{n,k}^\downarrow(0; x) = x^k(1-x)^{n-k}$.
346

347 These systems of differential equations can be rewritten as matrix differential equa-
348 tions with coefficient matrices Q and Q^\downarrow respectively. Because they are linear, first
349 order equations, they can be solved by matrix exponentiation. Because the expectation
350 of a polynomial in the Wright-Fisher diffusion remains a polynomial, the nested expecta-
351 tions can be computed via matrix multiplication of the solutions to these differential
352 equations, yielding the formula (2).

353 4.2 Sites covered exactly once have no information about drift 354 in the ancient population

355 Consider a simplified model in which each site has exactly one read. When we have
356 sequence from only a single individual, we have a set l_a of sites where the single read is
357 an ancestral allele and a set l_d of sites where the single read is a derived allele. Thus,
358 we can rewrite (3) as

$$L(D) = \prod_{l \in l_a} \left((1-\epsilon)P_{2,0}(x_l) + \frac{1}{2}P_{2,1}(x_l) + \epsilon P_{2,2}(x_l) \right) \prod_{l \in l_d} \left(\epsilon P_{2,0}(x_l) + \frac{1}{2}P_{2,1}(x_l) + (1-\epsilon)P_{2,2}(x_l) \right).$$

We can use formulas from Racimo et al. [2016] to compute $P_{2,k}(x_l)$ for $k \in \{0, 1, 2\}$,

$$\begin{aligned} P_{2,0}(x_l) &= 1 - x_l e^{-t_1} - \frac{1}{2}x_l e^{-(t_1+t_2)} + x_l \left(x_l - \frac{1}{2} \right) e^{-(3t_1+t_2)} \\ P_{2,1}(x_l) &= x_l e^{-(t_1+t_2)} + x_l (1 - 2x_l) e^{-(3t_1+t_2)} \\ P_{2,2}(x_l) &= x_l e^{-t_1} - \frac{1}{2}x_l e^{-(t_1+t_2)} + x_l \left(x_l - \frac{1}{2} \right) e^{-(3t_1-t_2)}. \end{aligned}$$

359 Note then that

$$(1 - \epsilon)P_{2,0}(x_l) + \frac{1}{2}P_{2,1}(x_l) + \epsilon P_{2,2}(x_l) = 1 - \epsilon - x(1 - 2\epsilon)e^{-t_1}$$

360 and

$$\epsilon P_{2,0}(x_l) + \frac{1}{2}P_{2,1}(x_l) + (1 - \epsilon)P_{2,2}(x_l) = \epsilon + x(1 - 2\epsilon)e^{-t_1}.$$

361 Neither of these formulas depend on t_2 ; hence, there is no information about the drift
362 time in the ancient population from data that is exactly 1x coverage.

363 5 Software Availability

364 Python implementations of the described methods are available at www.github.com/schraiber/continuity/

365 6 Acknowledgments

366 We wish to thank Melinda Yang, Iain Mathieson, Pontus Skoglund, and Fernando
367 Racimo for several discussions during the conception of this work that greatly improved
368 its scope and rigor. We are grateful to Fernando Racimo and Benjamin Vernot for
369 comments on early versions of this work that significantly improved its quality. We
370 would also like to thank Tamara Broderick for several stimulating discussions about
371 clustering that ultimately didn't result in any interesting application to ancient DNA.

372 References

373 David H Alexander, John Novembre, and Kenneth Lange. Fast model-based estimation
374 of ancestry in unrelated individuals. *Genome research*, 19(9):1655–1664, 2009.

375 Morten E Allentoft, Martin Sikora, Karl-Göran Sjögren, Simon Rasmussen, Morten
376 Rasmussen, Jesper Stenderup, Peter B Damgaard, Hannes Schroeder, Torbjörn

377 Ahlström, Lasse Vinner, et al. Population genomics of bronze age eurasia. *Nature*, 522(7555):167–172, 2015.

378

379 1000 Genomes Project Consortium. A global reference for human genetic variation. *Nature*, 526(7571):68–74, 2015.

380

381 Jesse Dabney, Matthias Meyer, and Svante Pääbo. Ancient dna damage. *Cold Spring Harbor perspectives in biology*, 5(7):a012567, 2013.

382

383 Warren J Ewens. *Mathematical population genetics 1: theoretical introduction*, volume 27. Springer Science & Business Media, 2012.

384

385 Daniel Falush, Lucy van Dorp, and Daniel Lawson. A tutorial on how (not) to over-interpret structure/admixture bar plots. *bioRxiv*, page 066431, 2016.

386

387 Qiaomei Fu, Cosimo Posth, Mateja Hajdinjak, Martin Petr, Swapan Mallick, Daniel Fernandes, Anja Furtwängler, Wolfgang Haak, Matthias Meyer, Alissa Mittnik, et al. The genetic history of ice age europe. *Nature*, 2016.

388

389

390 Richard E Green, Johannes Krause, Adrian W Briggs, Tomislav Maricic, Udo Stenzel, Martin Kircher, Nick Patterson, Heng Li, Weiwei Zhai, Markus Hsi-Yang Fritz, et al. A draft sequence of the neandertal genome. *science*, 328(5979):710–722, 2010.

391

392

393 RC Griffiths. The frequency spectrum of a mutation, and its age, in a general diffusion model. *Theoretical population biology*, 64(2):241–251, 2003.

394

395 Wolfgang Haak, Iosif Lazaridis, Nick Patterson, Nadin Rohland, Swapan Mallick, Bastien Llamas, Guido Brandt, Susanne Nordenfelt, Eadaoin Harney, Kristin Stewardson, et al. Massive migration from the steppe was a source for indo-european languages in europe. *Nature*, 522(7555):207–211, 2015.

396

397

398

399 Ethan M Jewett, Matthias Steinrücken, and Yun S Song. The effects of population size histories on estimates of selection coefficients from time-series genetic data. *Molecular Biology and Evolution*, page msw173, 2016.

400

401

John A Kamm, Jonathan Terhorst, and Yun S Song. Efficient computation of the joint sample frequency spectra for multiple populations. *Journal of Computational and Graphical Statistics*, (just-accepted):1–37, 2016.

Samuel Karlin and Howard E Taylor. *A second course in stochastic processes*. Elsevier, 1981.

Jerome Kelleher, Alison M Etheridge, and Gilean McVean. Efficient coalescent simulation and genealogical analysis for large sample sizes. *PLoS Comput Biol*, 12(5):e1004842, 2016.

Thorfinn Sand Korneliussen, Anders Albrechtsen, and Rasmus Nielsen. Angsd: analysis of next generation sequencing data. *BMC bioinformatics*, 15(1):356, 2014.

Iosif Lazaridis, Nick Patterson, Alissa Mittnik, Gabriel Renaud, Swapan Mallick, Karola Kirsanow, Peter H Sudmant, Joshua G Schraiber, Sergi Castellano, Mark Lipson, et al. Ancient human genomes suggest three ancestral populations for present-day europeans. *Nature*, 513(7518):409–413, 2014.

Iosif Lazaridis, Dani Nadel, Gary Rollefson, Deborah C Merrett, Nadin Rohland, Swapan Mallick, Daniel Fernandes, Mario Novak, Beatriz Gamarra, Kendra Sirak, et al. Genomic insights into the origin of farming in the ancient near east. *Nature*, 536(7617):419–424, 2016.

Mark Lipson and David Reich. Working model of the deep relationships of diverse modern human genetic lineages outside of africa. *Molecular Biology and Evolution*, page msw293, 2017.

Mark Lipson, Po-Ru Loh, Nick Patterson, Priya Moorjani, Ying-Chin Ko, Mark Stoneking, Bonnie Berger, and David Reich. Reconstructing austronesian population history in island southeast asia. *Nature communications*, 5, 2014.

Iain Mathieson, Iosif Lazaridis, Nadin Rohland, Swapan Mallick, Nick Patterson, Songül Alpaslan Roodenberg, Eadaoin Harney, Kristin Stewardson, Daniel Fernan-

des, Mario Novak, et al. Genome-wide patterns of selection in 230 ancient eurasians. *Nature*, 528(7583):499–503, 2015.

Matthias Meyer, Martin Kircher, Marie-Theres Gansauge, Heng Li, Fernando Racimo, Swapan Mallick, Joshua G Schraiber, Flora Jay, Kay Prüfer, Cesare De Filippo, et al. A high-coverage genome sequence from an archaic denisovan individual. *Science*, 338(6104):222–226, 2012.

Rasmus Nielsen, Thorfinn Korneliussen, Anders Albrechtsen, Yingrui Li, and Jun Wang. Snp calling, genotype calling, and sample allele frequency estimation from new-generation sequencing data. *PloS one*, 7(7):e37558, 2012.

Nick Patterson, Priya Moorjani, Yontao Luo, Swapan Mallick, Nadin Rohland, Yiping Zhan, Teri Genschoreck, Teresa Webster, and David Reich. Ancient admixture in human history. *Genetics*, 192(3):1065–1093, 2012.

Benjamin M Peter. Admixture, population structure, and f-statistics. *Genetics*, 202(4):1485–1501, 2016.

Joseph K Pickrell and Jonathan K Pritchard. Inference of population splits and mixtures from genome-wide allele frequency data. *PLoS Genet*, 8(11):e1002967, 2012.

Ron Pinhasi, Daniel Fernandes, Kendra Sirak, Mario Novak, Sarah Connell, Songül Alpaslan-Roodenberg, Fokke Gerritsen, Vyacheslav Moiseyev, Andrey Gromov, Pál Raczky, et al. Optimal ancient dna yields from the inner ear part of the human petrous bone. *PloS one*, 10(6):e0129102, 2015.

Jonathan K Pritchard, Matthew Stephens, and Peter Donnelly. Inference of population structure using multilocus genotype data. *Genetics*, 155(2):945–959, 2000.

Fernando Racimo, Gabriel Renaud, and Montgomery Slatkin. Joint estimation of contamination, error and demography for nuclear dna from ancient humans. *PLoS Genet*, 12(4):e1005972, 2016.

453 Morten Rasmussen, Sarah L Anzick, Michael R Waters, Pontus Skoglund, Michael De-
454 Giorgio, Thomas W Stafford Jr, Simon Rasmussen, Ida Moltke, Anders Albrechtsen,
455 Shane M Doyle, et al. The genome of a late pleistocene human from a clovis burial
456 site in western montana. *Nature*, 506(7487):225–229, 2014.

457 Susanna Sawyer, Johannes Krause, Katerina Guschanski, Vincent Savolainen, and
458 Svante Pääbo. Temporal patterns of nucleotide misincorporations and dna frag-
459 mentation in ancient dna. *PloS one*, 7(3):e34131, 2012.

460 Joshua G Schraiber, Steven N Evans, and Montgomery Slatkin. Bayesian inference of
461 natural selection from allele frequency time series. *Genetics*, 203(1):493–511, 2016.

462 Per Sjödin, Pontus Skoglund, and Mattias Jakobsson. Assessing the maximum con-
463 tribution from ancient populations. *Molecular biology and evolution*, page msu059,
464 2014.

465 Pontus Skoglund, Helena Malmström, Ayça Omrak, Maanasa Raghavan, Cristina
466 Valdiosera, Torsten Günther, Per Hall, Kristiina Tambets, Jüri Parik, Karl-Göran
467 Sjögren, et al. Genomic diversity and admixture differs for stone-age scandinavian
468 foragers and farmers. *Science*, 344(6185):747–750, 2014.

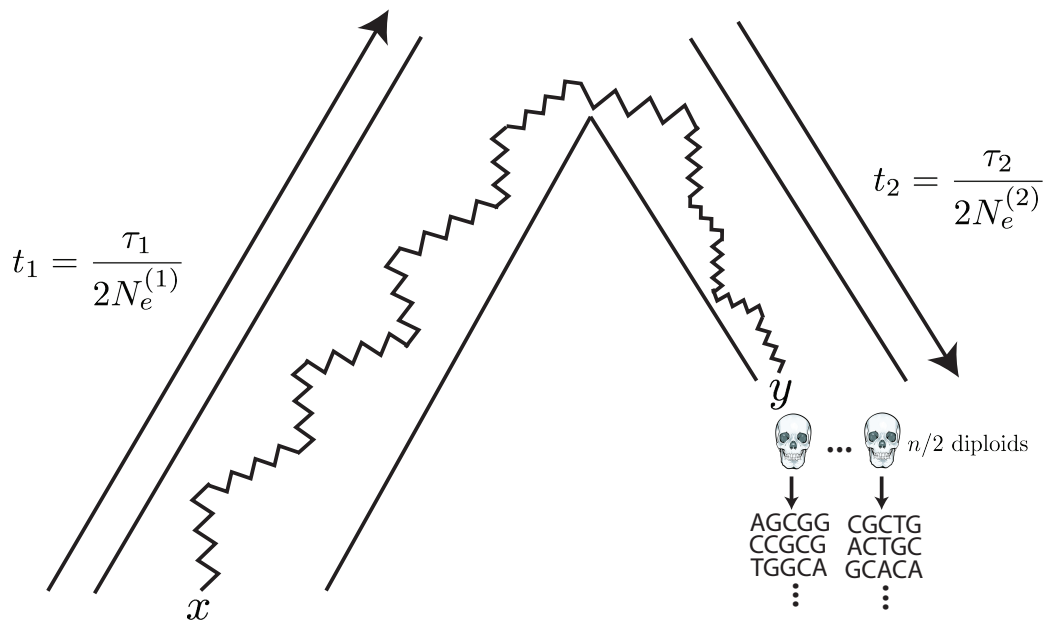


Figure 1: The generative model. Alleles are found at frequency x in the modern population and are at frequency y in the ancient population. The modern population has effective size $N_e^{(1)}$ and has evolved for τ_1 generations since the common ancestor of the modern and ancient populations, while the ancient population is of size $N_e^{(2)}$ and has evolved for τ_2 generations. Ancient diploid samples are taken and sequenced to possibly low coverage, with errors. Arrows indicate that the sampling probability can be calculated by evolving alleles *backward* in time from the modern population and then *forward* in time to the ancient population.

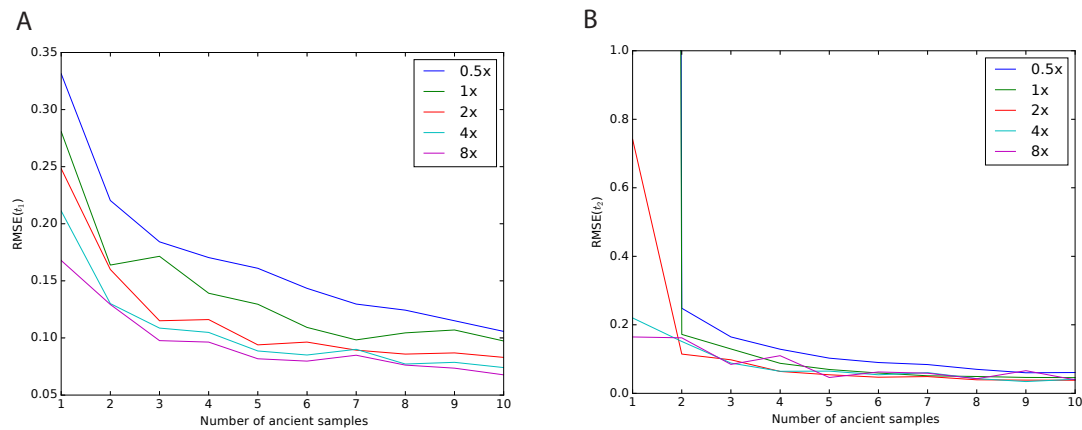


Figure 2: Impact of sampling scheme on parameter estimation error. In each panel, the x axis represents the number of simulated ancient samples, while the y axis shows the relative root mean square error for each parameter. Each different line corresponds to individuals sequenced to different depth of coverage. Panel A shows results for t_1 while panel B shows results for t_2 . Simulated parameters are $t_1 = 0.02$ and $t_2 = 0.05$.

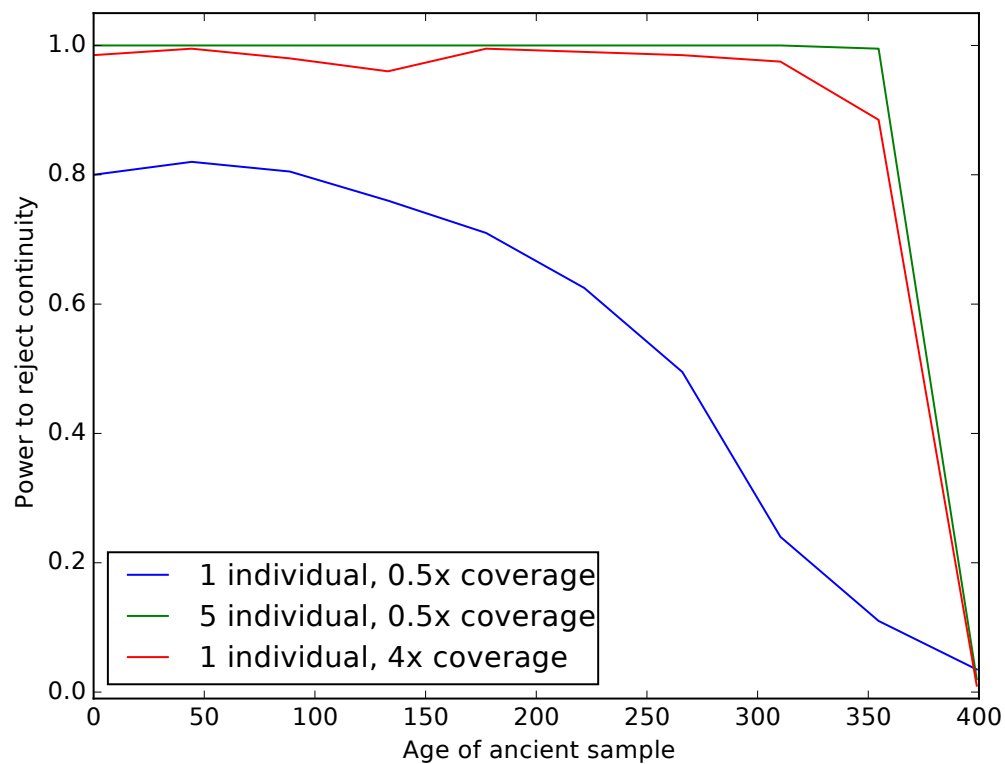


Figure 3: Impact of sampling scheme on rejecting population continuity. The x axis represents the age of the ancient sample in generations, with 0 indicating a modern sample and 400 indicating a sample from exactly at the split time 400 generations ago. The y axis shows the proportion of simulations in which we rejected the null hypothesis of population continuity. Each line shows different sampling schemes, as explained in the legend.

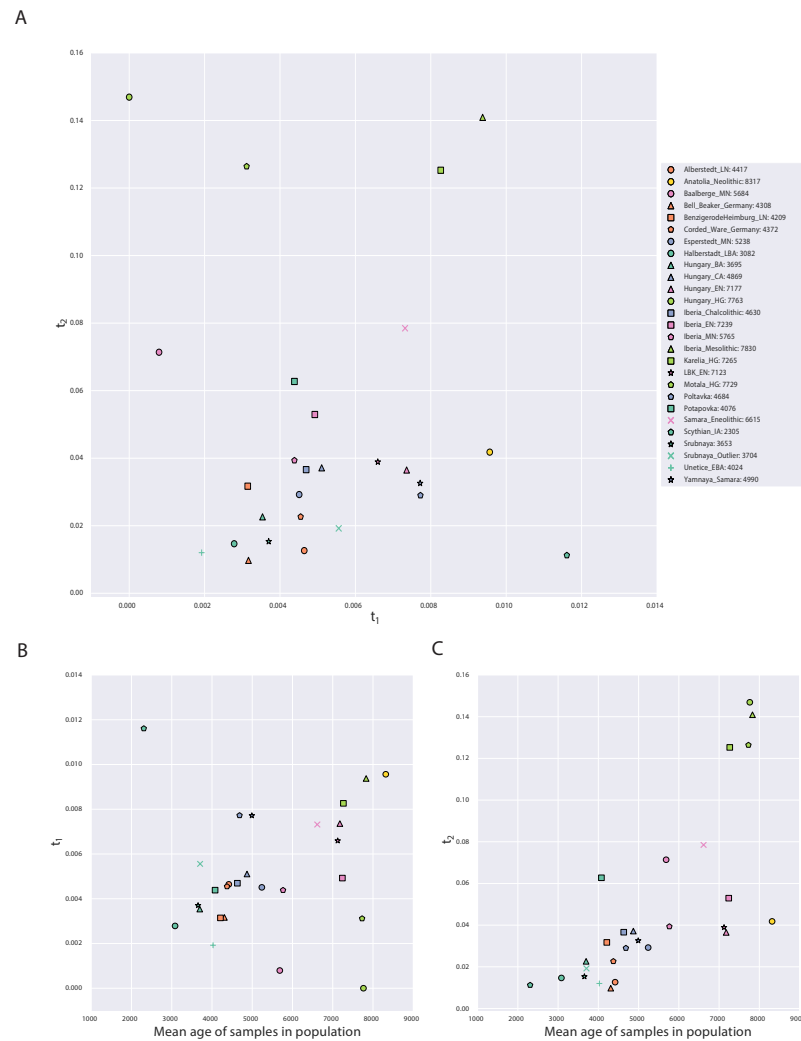


Figure 4: Parameters of the model inferred from ancient West Eurasian samples. Panel A shows t_1 on the x-axis and t_2 on the y-axis, with each point corresponding to a population as indicated in the legend. Numbers in the legend correspond to the mean date of all samples in the population. Panels B and C show scatterplots of the mean age of the samples in the population (x-axis) against t_1 and t_2 , respectively. Points are described by the same legend as Panel A.

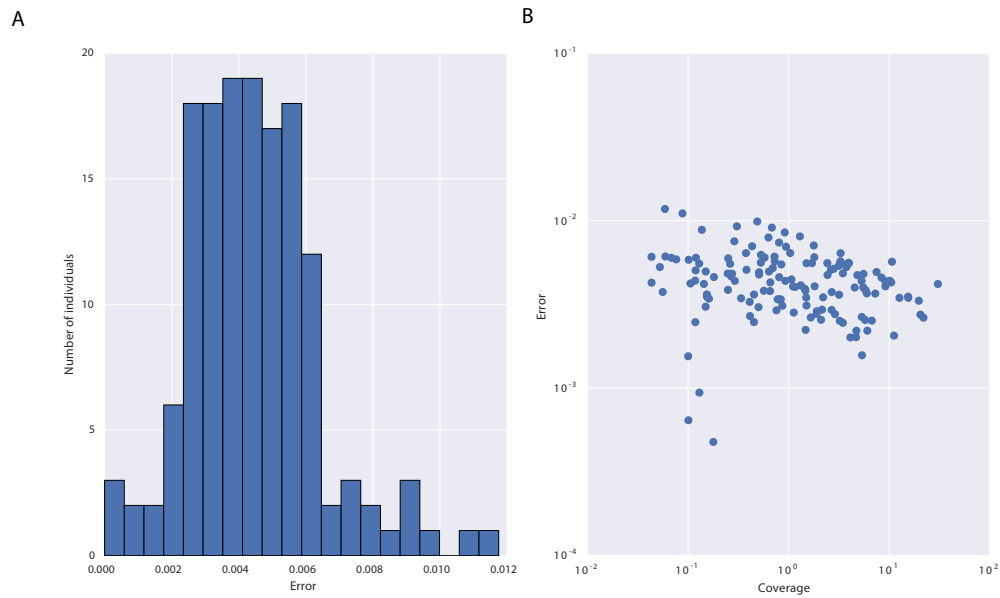


Figure 5: Properties of sequencing error inferred from ancient samples. Panel A shows a histogram of error rates estimated across all samples. Panel B is a scatterplot of coverage (x-axis) against inferred error rate (y-axis) for all individuals, except two individuals for whom an error rate of 0 was estimated.

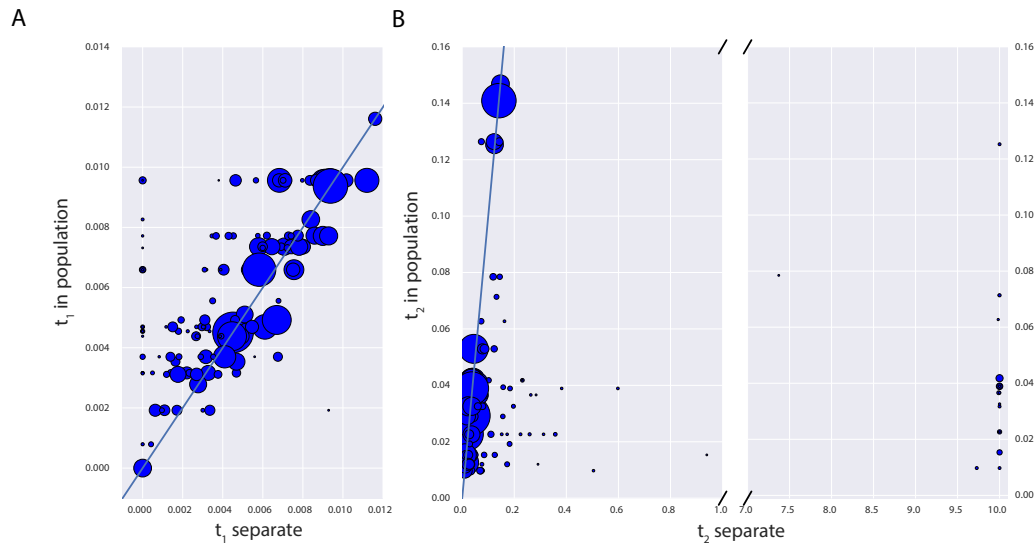


Figure 6: Impact of pooling individuals into populations when estimating model parameters from real data. In both panels, the x-axis indicates the parameter estimate when individuals are analyzed separately, while the y-axis indicates the parameter estimate when individuals are grouped into populations. Size of points is proportional to the coverage of each individual. Panel A reports the impact on estimation of t_1 , while Panel B reports the impact on t_2 . Note that Panel B has a broken x-axis. Solid lines in each figure indicate $y = x$.

pop	cov	date	t_1	t_2	lnL	t_1 (cont)	lnL (cont)
Alberstedt_LN	12.606	4417.000	0.005	0.013	-779411.494	0.006	-779440.143
Anatolia_Neolithic	3.551	8317.500	0.010	0.042	-9096440.714	0.044	-9106156.877
Baalberge_MN	0.244	5684.333	0.001	0.071	-201575.306	0.007	-201750.419
Bell_Beaker_Germany	1.161	4308.444	0.003	0.010	-1834486.744	0.008	-1834652.858
BenzigerodeHeimburg_LN	0.798	4209.750	0.003	0.032	-346061.545	0.007	-346134.356
Corded_Ware_Germany	2.250	4372.833	0.005	0.023	-2139002.723	0.017	-2139858.192
Esperstedt_MN	30.410	5238.000	0.005	0.029	-975890.329	0.009	-976047.889
Halberstadt_LBA	5.322	3082.000	0.003	0.015	-558966.522	0.004	-558993.078
Hungary_BA	3.401	3695.750	0.004	0.023	-789754.969	0.010	-789939.889
Hungary_CA	5.169	4869.500	0.005	0.037	-504413.094	0.010	-504549.603
Hungary_EN	4.033	7177.000	0.007	0.036	-3478429.262	0.033	-3481855.461
Hungary_HG	5.807	7763.000	0.000	0.147	-469887.471	0.015	-471652.083
Iberia_Chalcolithic	1.686	4630.625	0.005	0.037	-2351769.869	0.028	-2354249.543
Iberia_EN	4.875	7239.500	0.005	0.053	-1483274.628	0.030	-1485675.934
Iberia_MN	5.458	5765.000	0.004	0.039	-1491407.962	0.023	-1492793.179
Iberia_Mesolithic	21.838	7830.000	0.009	0.141	-720759.133	0.030	-723091.935
Karelia_HG	2.953	7265.000	0.008	0.125	-652952.676	0.033	-655352.439
LBK_EN	2.894	7123.429	0.007	0.039	-3656617.954	0.033	-3660838.639
Motala_HG	2.207	7729.500	0.003	0.126	-1477338.076	0.068	-1489573.895
Poltavka	2.211	4684.500	0.008	0.029	-1334662.071	0.020	-1335358.630
Potapovka	0.267	4076.500	0.004	0.063	-220112.816	0.011	-220251.379
Samara_Eneolithic	0.463	6615.000	0.007	0.078	-362161.674	0.020	-362689.209
Scythian_IA	3.217	2305.000	0.012	0.011	-492961.306	0.013	-492973.694
Srubnaya	1.662	3653.273	0.004	0.015	-2578065.957	0.013	-2578645.731
Srubnaya_Outlier	0.542	3704.500	0.006	0.019	-285828.766	0.008	-285851.523
Unetice_EBA	1.320	4024.786	0.002	0.012	-1676798.610	0.008	-1677026.310
Yamnaya_Samara	1.937	4990.500	0.008	0.033	-2440183.354	0.028	-2442192.801

Table 1: Details of populations included in analysis. “pop” is population name, “cov” is mean coverage of individuals in the population, “date” is mean date of individuals in the population, “ t_1 ” is the maximum likelihood estimate of t_1 in the full model, “ t_2 ” is the maximum likelihood estimate of t_2 in the full model, “LnL” is the maximum likelihood value in the full model, “ t_1 (cont)” is the maximum likelihood estimate of t_1 in the model where $t_2 = 0$, “LnL” is the maximum likelihood value in the model where $t_2 = 0$.